PCCP

PAPER

View Article Online
View Journal | View Issue

Cite this: *Phys. Chem. Chem. Phys.*, 2017, **19**, 29812

Sub-Doppler infrared spectroscopy of resonance-stabilized hydrocarbon intermediates: ν_3/ν_4 CH stretch modes and CH_2 internal rotor dynamics of benzyl radical†

A. Kortyna,[a] A. J. Samin,[b] T. A. Miller[b] and D. J. Nesbitt*[acd]

Received 24th August 2017,
Accepted 16th October 2017

DOI: 10.1039/c7cp05776h

rsc.li/pccp

Highly reactive benzyl radicals are generated by electron dissociative attachment to benzyl chloride doped into a neon–hydrogen–helium discharge and immediately cooled to T_{rot} = 15 K in a high density, supersonic slit expansion environment. The sub-Doppler spectra are fit to an asymmetric-top rotational Hamiltonian, thereby yielding spectroscopic constants for the ground (v = 0) and first excited (v = 1, ν_3, ν_4) vibrational levels of the ground electronic state. The rotational constants obtained for the ground state are in good agreement with previous laser induced fluorescence measurements (LIF), with vibrational band origins (ν_3 = 3073.2350 ± 0.0006 cm^{-1}, ν_4 = 3067.0576 ± 0.0006 cm^{-1}) in agreement with anharmonically corrected density functional theory calculations. To assist in detection of benzyl radical in the interstellar medium, we have also significantly improved the precision of the ground state rotational constants through combined analysis of the ground state IR and LIF combination differences. Of dynamical interest, there is no evidence in the sub-Doppler spectra for tunneling splittings due to internal rotation of the CH_2 methylene subunit, which implies a significant rotational barrier consistent with partial double bond character in the CC bond. This is further confirmed with high level *ab initio* calculations at the CCSD(T)-f12b/ccpVdZ-f12 level, which predict a zero-point energy corrected barrier to internal rotation of $\Delta E_{tun} \approx$ 11.45 kcal mol^{-1} or 4005 cm^{-1}. In summary, the high-resolution infrared spectra are in excellent agreement with simple physical organic chemistry pictures of a strongly resonance-stabilized benzyl radical with a nearly rigid planar structure due to electron delocalization around the aromatic ring.

I. Introduction

The benzyl radical is a textbook example of resonantly stabilized, open shell organic species, with multiple "resonance structures" due to facile electron delocalization and rehybridization around the aromatic ring. Such resonant stabilization effects translate into an unusually low free energy, which in turn is responsible for making benzyl radical a relatively long-lived and therefore especially abundant transient intermediate in aromatic hydrocarbon chemistry. Systems of particular relevance are the combustion of fossil fuels, especially in the formation kinetics of polycyclic aromatic hydrocarbons (PAH) and, eventually, particulate soot.[1] Resonantly stabilized radicals are produced in sooty combustion environments,[2,3] and benzyl radicals are readily formed from reactions of small hydrocarbons.[4] It is known that formation of bibenzyl from two benzyl radicals is barrierless,[5] with several pathways leading from benzyl to three-ring aromatics studied by Sinha and Raj.[6]

Interest in the benzyl radical is also partly fueled by the desire to probe the nature of its multiple equivalent resonance structures. For benzyl, simple freshman chemistry teaches us that the unpaired radical center can be localized on any of 3 locations: the CH_2 subunit (in two different Kekule structures) or on the one *para*- and two *ortho*-positions on the aromatic ring.[7] This leads to a total of five nearly equivalent structures describing the benzyl radical ground electronic state,[8] whose additional uncertainty in the radical electron location results in

[a] *JILA, National Institute of Standards and Technology, University of Colorado, Boulder, Colorado 80309, USA*
[b] *Department of Chemistry and Biochemistry, The Ohio State University, Columbus, Ohio 43210, USA*
[c] *Department of Physics, University of Colorado Boulder, Boulder, CO 80309, USA*
[d] *Department of Chemistry and Biochemistry, University of Colorado, Boulder, Colorado 80309, USA*

† Electronic supplementary information (ESI) available: To help facilitate and coordinate reliable predictions required for astronomical search efforts towards benzyl in the microwave/mm wave region, we have included 6 tables of ESI.† Table I and II list the 2-line combination differences used in the least squares fits for the ground state molecular constants, with Table I containing only the sub-Doppler IR data from JILA and Table II representing the combined set from the Nesbitt and Miller groups. Similarly, Tables III and IV provide obs., calc., and (obs-calc) transition frequencies from least squares fits for the ν_3 band, with ground state constants fixed at the values obtained in Tables I and II, respectively. Likewise, Tables V and VI provide obs., calc., and (obs-calc) transition frequencies from least squares fits for the ν_4 band, with ground state constants fixed at the values obtained in Tables I and II, respectively. See DOI: 10.1039/c7cp05776h

resonance stabilization. Interestingly, the latter radical configurations noted above, *i.e.*, with the unpaired electron localized on either the *ortho*- or *para*-carbon atoms, imparts partial olefinic (sp^2) character to the nominally CC (sp^3 hybridized) toluyl bond. Such double bond character can dramatically increase the barrier to internal rotation, thereby dramatically reducing the density of states for a given internal vibrational energy. This can therefore significantly impact the extent of intramolecular coupling of such hindered rotor states with other vibrational modes, and thus the time scale and/or high resolution spectral evidence for important unimolecular dynamics such as intramolecular vibrational redistribution (IVR).[9]

By virtue of the low electronic states made possible by resonance delocalization, the benzyl radical has been particularly well studied in the UV-visible region of the spectrum.[10] This species was first observed in emission by Schüler *et al.*[11] and by fluorescence generated *via* photolysis of toluene by Porter and Strachan.[12] Dispersed emission spectroscopy was used to determine the C_{2v} symmetries for the ground and first two excited electronic states,[13,14] with laser induced fluorescence (LIF) methods subsequently exploited for examining the rotationally resolved spectroscopy[3,15] to high precision by Lin *et al.*[16] More recently, multiple electronically excited states have been studied using cavity ring-down spectroscopy,[17] with electronic structure calculations computed using high level *ab initio* quantum chemical methods.[18]

With respect to the vibrational structure and spectroscopy for the ground electronic state of benzyl radical, much less is known. Indeed, there has been only one matrix isolation infrared (IR) study of the vibrational bands of benzyl radical in an argon matrix;[19] specifically, Baskir *et al.*[19] report the position of 15 band origins, including the ν_4 CH stretch band investigated at much higher resolution in the present work. The symmetry of the ground electronic state has been determined to be $^2B_2$ in the C_{2v} point group (for example, see ref. 18), which transforms like a vector normal to the molecular plane.

In the present work, we have investigated two CH stretch modes of the benzyl radical associated with the aromatic ring. For consistency with the literature, we adopt the notation of Lineberger *et al.*, whereby the normal modes are simply numbered in order of decreasing frequency.[20] In this numbering scheme, the vibrational modes observed are labeled ν_3 and ν_4. As illustrated in Fig. 1a, the ν_3 mode reflects the "in-phase" component of the antisymmetric CH stretch of the aromatic ring, with its transition dipole moment lying along the *B* inertial axis. This mode has a B_2 vibrational symmetry in the C_{2v} point group, with IR transitions from the ground state reflecting b-type selection rules (ΔK_a and $\Delta K_c = \pm1, \pm3$, *etc.*) and K_a, K_c denoting approximate projections of the total angular momentum along the *A* and *C* axes, respectively. At slightly lower energy is the ν_4 mode, which corresponds to the "in-phase" component of the symmetric CH stretch of the aromatic ring (see Fig. 1b). The ν_4 transition dipole moment lies along the molecular A (+*z*) axis (*i.e.*, along the CC toluyl bond) and thus transitions from the ground state reflect a-type selection rules ($\Delta K_a = 0, \pm2$, *etc.* and $\Delta K_c = \pm1, \pm3$, *etc.*).

The organization of this paper is as follows. Section II describes the apparatus and experimental procedure, with the spectroscopic results presented in Section III. Section IV provides a more detailed analysis of the spectroscopic information, including high level *ab initio* calculations of barrier heights to internal rotation, tunneling splittings, and evidence for a remarkably small degree of coupling to a high density of background ("dark") states. Concluding remarks are summarized in Section V.

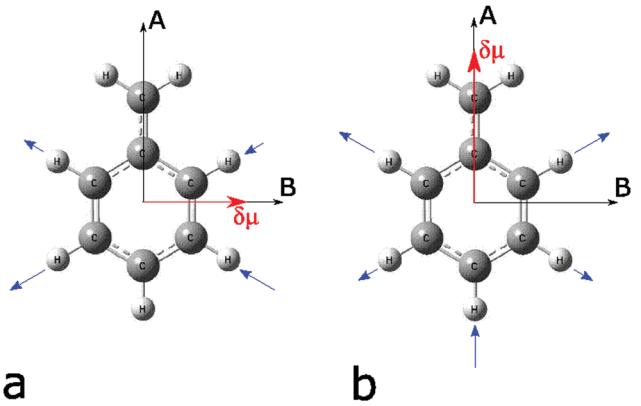

Fig. 1 Structure of benzyl radical, with *A* and *B* indicating principal axes with the smallest and intermediate moments of inertia, respectively. The atoms undergoing significant displacement for each vibrational mode studied (ν_3 in panel a, ν_4 in panel b) are highlighted by blue arrows with lengths reflecting their relative CH stretch displacement, with the net transition dipole moments, $\delta\mu$, indicated as well.

II. Experiment

The supersonic slit-discharge IR absorption spectrometer has been described in detail elsewhere,[21] with only a brief overview necessary here. Narrow band (<1 MHz) tunable IR radiation is produced by difference frequency generation of a ring dye laser and a single mode Ar^+ laser in a periodically poled $LiNbO_3$ (PPLN) crystal[22] with 1 mm × 40 mm × 10 mm dimensions and 12 poling periods. Quasi-phase matching is achieved *via* precise temperature control of the PPLN crystal in a temperature stabilized oven ($\Delta T = 0.1$ °C), with the two laser beams spatially overlapped in a soft focus (approximately 60 μm waist) over the full 40 mm length. With 180 mW of rhodamine 590 dye and 300 mW of Ar^+ (514.5 nm line), frequency difference generation in PPLN is capable of producing 15–20 μW of narrow band IR radiation that can be tuned between 2600 cm^{-1} and 3450 cm^{-1}.

After the PPLN crystal, the remaining visible light is filtered from the IR beam and a beamsplitter reflects roughly 50% of the IR light onto a liquid-nitrogen cooled InSb (reference) detector. The reference detector output is sampled by a fast subtraction circuit which cancels common-mode laser amplitude noise by >30 dB in a 1 MHz bandwidth. The other half of the IR beam passes into a vacuum chamber containing a 16-pass Herriott cell at the throat of the slit-discharge pulsed molecular beam source. The 300 μm slit width × 4 cm slit length, combined with a Herriott multipass cell yields a 64 cm path length of the IR beam through the absorbing species in the slit expansion region, after which the unattenuated IR

radiation passes onto a second liquid-nitrogen cooled InSb (signal) detector.

The slit molecular beam source operates at 19 Hz with a 1000 μs pulse width. The backing pressure of about 200 mbar is provided by a 52% neon, 25% hydrogen, and 23% helium carrier gas mixture. The benzyl chloride precursor is seeded into the carrier gas at a maximum 0.4% total concentration by bubbling the carrier gas through a temperature controlled liquid sample of benzyl chloride. Benzyl radical is formed by cleaving of the C–Cl bond in the slit discharge, largely through dissociative attachment with free electrons in the plasma environment. The supersonic expansion cools the benzyl radicals to about 15 K, insuring a high density of radicals per quantum state.

The discharge is struck by applying a 7.0 kV cm^{-1} 50 kHz square wave electric field between the body of the pulsed valve and a set of electrodes that define the beam source aperture, generating peak discharge currents I_{max} = 500 mA. We estimate a radical density of 1.0×10^{12} radicals per cm^3 about 5 mm downstream of the slit nozzle orifice. This estimate is based on the measured spectra, the residual sub-Doppler linewidth (60 MHz), and IR integrated absorption coefficients computed from a density function theory (DFT) B3LYP calculation[23] using a 6-311G++(3df,3pd) basis set. The 50 kHz discharge modulates the radical absorption signal, which is subsequently analyzed by phase-sensitive, lock-in detection with a fast (100 μs) time constant. The demodulated signal is passed through a gated integrator for background subtraction, digitized, and stored in computer memory for later plotting and spectral analysis. By virtue of the lock-in detection and balanced cancellation of technical laser amplitude noise, this procedure yields high quality, direct absorption spectra with rms absorbance noise levels $\left(1.5 \times 10^{-6} \text{ per } \sqrt{\text{Hz}}\right)$ within a factor of two of the quantum "shot-noise" limit on the incident IR photon flux.

The high frequency resolution of this experiment is crucially dependent on an actively stabilized Fabry–Pérot optical transfer cavity with a 250 MHz free spectral range. The length of this Fabry–Pérot cavity is locked to a single fringe of a frequency stabilized HeNe laser (see Riedle *et al.*[24] for details). In turn, the frequency of the single-mode Ar^+ laser is locked to one fringe of the same Fabry–Pérot cavity, effectively transferring the stability of the HeNe laser to the Ar^+ laser. The relative frequency of the dye laser is determined by counting its fringes transmitted through the transfer cavity. In practice, the relative IR frequency is reproducible to within ±11 MHz or $\pm 4 \times 10^{-4}$ cm^{-1}. The absolute IR frequency is referenced to four previously measured CH_4 lines in the nearby ν_3 R(4) manifold,[25] which we can determine to an uncertainty of ±7 MHz ($\pm 2 \times 10^{-4}$ cm^{-1}) from Gaussian fits to their absorption profiles, providing an absolute accuracy of ±15 MHz ($\pm 5 \times 10^{-4}$ cm^{-1}) for any individual spectral feature for benzyl radical.

III. Results and analysis

High-resolution IR spectra are collected from 3064 cm^{-1} to 3078 cm^{-1}. We ensure reproducibility by measuring the position of any assigned spectral feature a minimum of three times. The integrated IR intensity of the ν_3 mode is estimated to be a factor of 5.5 greater than that for the ν_4 mode (46 km $mole^{-1}$ for the ν_3 mode compared to 8.4 km $mole^{-1}$ for the ν_4 mode as determined by a DFT B3LYP calculation using the 6-311G++(3df,3dp) basis set). For the ν_3 band, the P and R branches account for almost all of the integrated IR intensity, whereas for the ν_4 mode, most of the integrated IR intensity is tied up in an unresolved, slightly red shaded Q branch. This, combined with the lower IR intensity, makes the signal level for the ν_4 P and R branches relatively small. To compensate for the low signal-to-noise ratio of the P and R branch, the ν_4 spectrum (3064 cm^{-1} to 3069.5 cm^{-1}) is averaged for 64 gas pulses (at roughly 1 ms duration per pulse) at each frequency point, whereas sufficient signal-to-noise in the ν_4 spectrum (3069.5 cm^{-1} to 3078 cm^{-1}) only requires averaging for 4 gas pulses per point. Fig. 2 shows the entire spectrum scanned for this report, and the effect of increased averaging can be seen in the ν_4 band, whose noise level is pushed down to roughly 2×10^{-7} per $\sqrt{\text{Hz}}$ rms absorbance sensitivity.

The benzyl data are analyzed by fitting isolated peaks in the rotationally resolved spectra to an asymmetric top Watson Hamiltonian[26] based on a rigid, prolate asymmetric top model. This spectral analysis has been tested two ways. First, we exploit in-house Fortran software programs to diagonalize the asymmetric rotor Hamiltonian in a Wang basis set,[27] using the resulting eigenvalues in a nonlinear weighted least-squares fit (STARPAC) to the spectra. Second, and by way of confirmation, we can take advantage of the remarkably powerful spectral

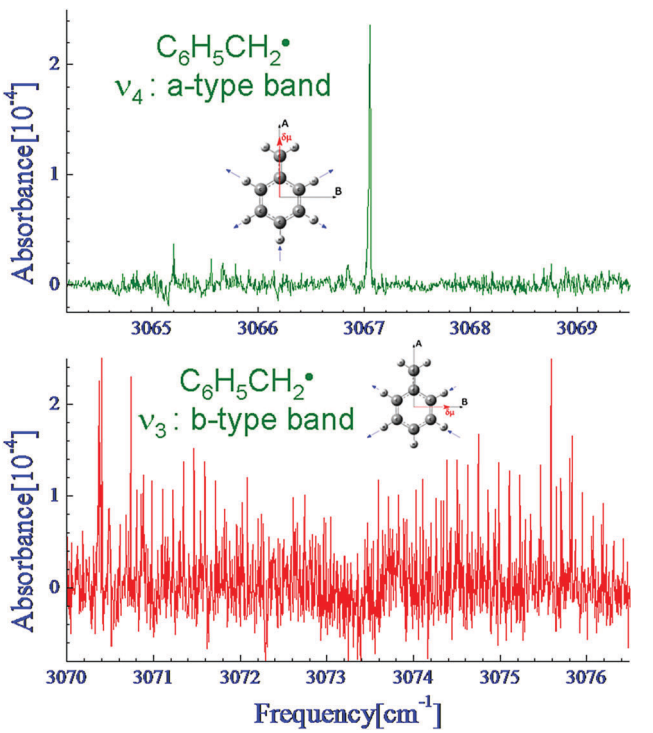

Fig. 2 Upper plot: The a-type transition from the ground state to the first excited (ν_4 = 1) vibrational mode, with 64 ms per pt averaging (64 gas pulses) and $\approx 0.8 \times 10^{-5}$ rms absorbance noise. Lower plot: The b-type transition from the ground to the first excited (ν_3 = 1) vibrational state, with 4 ms per pt averaging (4 gas pulses) and 5×10^{-5} rms absorbance noise.

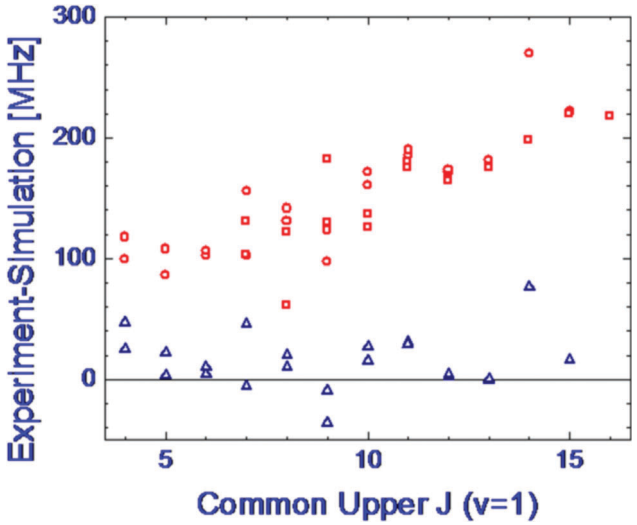

Fig. 3 Deviations between two-line combination differences and predictions from Lin *et al.*[16] The squares (circles) show the deviations between our data for the ν_3 (ν_4) band and two-line combination differences generated from previously published rotational constants.[16] The average deviation is 180 ± 10 MHz (140 ± 20 MHz), which can be clearly seen to grow linearly with rotational angular momentum. The triangles show corresponding deviations solely for two-line ground state combination differences between the IR ν_3 and ν_4 data, which yield a much smaller average deviation of 4 ± 9 MHz, *i.e.*, zero within statistical uncertainty.

simulation and least-squares fitting programs of PGOPHER written by Colin Western.[28,29] Gratifyingly, both approaches give results which are internally consistent within all reported statistical uncertainties.

We begin the analysis by verifying our spectral assignments using ground state two-line combination differences, and comparing these two-line combination differences to those generated using previously published rotational constants.[16] When our two-line combination differences are subtracted from those generated from the published rotation constants, we find small but systematic deviations as large as 200 MHz, *i.e.*, 18-fold larger than our experimental accuracy (see Fig. 3). In fact, this comparison reveals a trend of increasing deviation, ranging from approximately 100 MHz at low J to approximately 200 MHz at high J. As we shall see below, the differences between published rotational constants and the fits to our data are small ($<1\sigma$), but indeed large enough to introduce inconstancies into our attempts to fit the rotational constants for the upper states.

We circumvent this problem by generating our own ground state spectroscopic constants from our two-line combination differences. To check the consistency between the two-line combinations difference for the two vibrational modes, we fit spectroscopic constants to the two-line combination differences for the ν_3 band, and used these spectroscopic constants to generate a simulated spectrum for the ν_3 transition. Fig. 3 compares the measured ν_3 two-line combination differences to simulated two-line combination differences computed from the ν_3 ground state spectroscopic constants. The variation between these two sets of combination differences shows an average deviation of 4 ± 9 MHz, which is statistically indistinguishable from zero and well within the frequency precision of 11 MHz anticipated for the slit jet spectrometer apparatus.

Once this consistency was verified, we were able to assign 103 ground state two-line combination difference pairs for $K_a = 0 \leftarrow 0$, $1 \leftarrow 1$, and $2 \leftarrow 2$ transitions using both the ν_3 and ν_4 data, to which we applied our rigid-rotor Hamiltonian-diagonalization and eigenvalue fitting routines to generate robust, ground state high resolution A'', B'', and C'' spectroscopic constants. These fitted parameters are presented in Table 1 along with previously published (measured and computed) values, with which our results are in quite reasonable agreement. In comparison to the most precise of the previously published values,[29] the differences are all within 1σ, although some of the earlier published results show statistically significant differences, especially for the C rotational constant.

Next, we evaluate the excited state spectroscopic constants, obviously fixing the ground state parameters at the values reported in the first row of Table 1. For these fits, we use 117 $K_a = 1 \leftarrow 0$, $0 \leftarrow 1$, and $1 \leftarrow 2$ observed transitions from the ν_3 band and 94 $K_a = 0 \leftarrow 0$, $1 \leftarrow 1$, and $2 \leftarrow 2$ observed transitions for the ν_4 band. (See ESI† for a list of frequencies.) The uncertainties in the band origins, ν_0, reflect quadrature combinations of statistical uncertainties from the fitting routine and systematic uncertainties from the IR frequency accuracy (see Section II). Our band origin for the ν_3 band is appreciably blue shifted with respect to a previous argon matrix measurement (3069 cm^{-1}),[19] which likely reflects red shifts induced by the argon matrix. Both of our ν_0 measurements are within 1σ of the computed anharmonic values: $\nu_0 = 3062 \pm 10$ cm^{-1} for the ν_3 mode and $\nu_0 = 3077 \pm 10$ cm^{-1} for the ν_4 mode. These anharmonic vibrational frequencies are generated by calculating harmonic frequencies with a DFT/B3LYP method, and scaling the harmonic values by 0.9637 ± 0.0031 according to ref. 30.

The quality of these fits is illustrated in Fig. 4 for the ν_3 band and Fig. 5 for the ν_4 band. Both figures show details of the respective P branches, along with a simulated spectrum generated with the spectroscopic constants presented in Table 1 (first row)

Table 1 Spectroscopic constants of the $^2B_2$ ($v = 0$) ground state of benzyl radical. Units are cm^{-1} and the uncertainty in the least significant digit is shown in parentheses. Included are values generated with the following methods: supersonic jet—laser induced fluorescence (SSJ-LIF), Corona Excited Supersonic Expansion (CESE), multi-configuration self-consistent field calculation (MCSCF), Rotational Contour Analysis (RCA). The spectroscopic constants labeled as combined are generated with two-line combination differences from the present high resolution infrared data and previous lower resolution LIF results[16,46]

	A''	B''	C''
Present	0.1842(6)	0.09021(12)	0.0605251(16)
SSJ-LIF[16]	0.18416(5)	0.09013(3)	0.06051(2)
SSJ-LIF[15]	0.1841	0.0902	0.0604
CESE[14]	0.18484(10)	0.09007(5)	0.06046(4)
MCSCF[18]	0.18308	0.08963	0.06028
RCA[13]	0.1831	0.0909	0.0607
Combined	*0.18419(10)*	*0.09021(2)*	*0.0605259(13)*

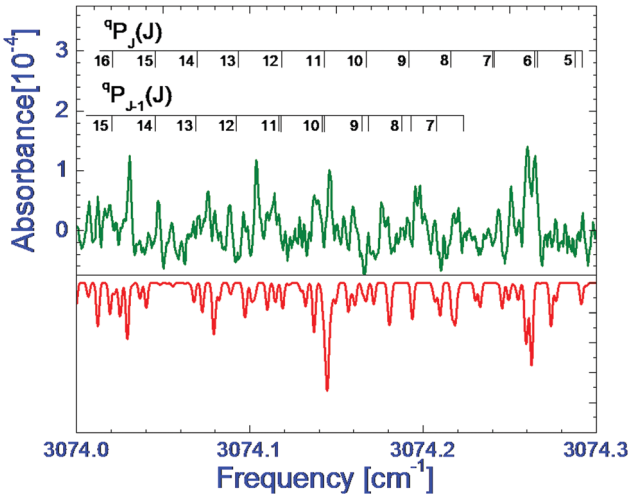

Fig. 4 Top panel: A detailed section of the ν_3 $^qP_K(J)$ ($K_c = J$ and $K_c = J - 1$) subbranches, with the $K_a = 1 \leftarrow 0$, $0 \leftarrow 1$, $2 \leftarrow 1$ and $1 \leftarrow 2$ asymmetry split progressions labeled. Bottom panel: Simulated spectrum assuming a 15 K rotational temperature, 60 MHz instrumental linewidth, and using the best fit spectroscopic constants given in Table 1 (first row) and Table 2 (first row).

and Table 2. Both figures also label the assigned progressions used in the fit that fall within the range of the figures. Transitions for K_a = 0, 1, and 2 for both bands are clearly reproduced by the simulations. There are also transitions out of levels with $K_a > 2$, but lower signal to noise complicated the assignment of these progressions, and thus were not included in any fit. There are also clear indications of small perturbations. For example, the blended

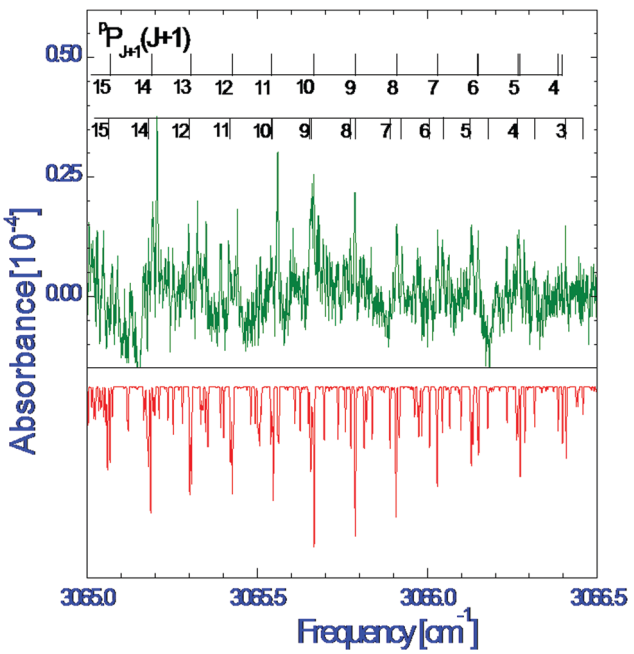

Fig. 5 Top panel: A detailed section of the ν_4 $^pP_{K=J}(J)$ b-type subbranches, with the $K_a = 0 \leftarrow 0$, $1 \leftarrow 1$, and $2 \leftarrow 2$ progressions labeled. Bottom panel: Simulated spectrum assuming a 15 K rotational temperature, 60 MHz instrumental linewidth, and the best fit spectroscopic constants given in Table 1 (first row) and Table 2 (second row).

Table 2 Spectroscopy constants and band origins of the ν_3 and ν_4 vibrationally excited states (v = 1) of the $^2B_2$ ground electronic state of benzyl radical, based on fits to the current high resolution infrared data. Units are cm^{-1} and the uncertainty in the least significant digit is shown in parentheses

	A'	B'	C'	ν_0
ν_3	0.1810(5)	0.09062(10)	0.060508(3)	3073.2350(6)
ν_4	0.18411(19)	0.09013(4)	0.060563(5)	3067.0576(8)

$13_{0,13} \leftarrow 14_{1,14}$ and $13_{1,13} \leftarrow 14_{0,14}$ lines for the ν_3 band, appear to be shifted by about -0.004 cm^{-1} (-120 MHz) from the predicted position, *i.e.*, by as much as twice the sub-Doppler linewidth and an order of magnitude more than the frequency reproducibility of the experiment.

IV. Discussion

A. Rovibrational analysis

The results in Table 2 indicate that vibrational motion has small but significant effects on the rotational constants for the ν_3 mode but not the ν_4 mode. Combining the experimental uncertainties in quadrature, compared to the ground state the ν_3 rotational constants change by 5σ–7σ, with A increasing by 1.7% and B decreasing by 0.45%. The C constant decreases by only 0.012%, although this is a statistically significant change. For the ν_4 vibrational mode, the rotational constants are statistically unchanged. This points toward the asymmetric CH stretch of the aromatic ring having a more profound effect on the molecular geometry than the symmetric CH stretch.

The rotational constants that we measure and present in Tables 1 and 2 are fitted using only P and R lines. For the ν_3 manifold, the Q branches are not intense enough to be detected with our instrumentation. For the ν_4 manifold, the Q branch is by far the most intense feature, but it is largely unresolved and therefore no unambiguous assignments can be made. However, the strong ν_4 Q branch can serve as a final check on the validity of the ν_4 spectroscopic constants. Fig. 6 shows the details of the ν_4 Q branch along with a simulation using our fitted spectroscopic constants for the ground state (Table 1, row 1) and the excited states (Table 2, row 2). Based on a typical 15 K rotational temperature and a 60 MHz instrumental linewidth, there is indeed quite good agreement between the data and the simulation, in particular, capturing a subtle red shading of the highly overlapped Q-branch spectral feature.

B. Intramolecular vibrational coupling

One question of particular relevance is whether or not such a large, polyatomic species as the benzyl radical would even exhibit a substantially rotationally resolved spectrum at high spectral resolution. Indeed, benzyl radical has 36 vibrational modes, which leads one to anticipate a high density of rovibrational states at 3000 cm^{-1} of internal excitation. Furthermore, we are exciting high frequency CH stretches, with a well-known propensity for 2 : 1 Fermi resonance coupling with the CH bend manifold. Intuition suggests that the density of states in the

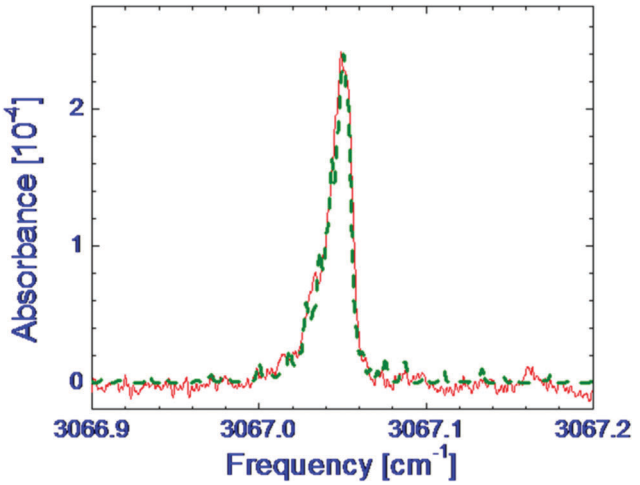

Fig. 6 Detailed comparison of the ν_4 Q branch (solid line) with a 15 K p-gopher simulation convoluted with a 60 MHz instrumental linewidth (dashed line). The simulation uses spectroscopic constants in Table 1 (first row) and Table 2 (second row) derived by fitting the eigenvalues of the rigid-rotor asymmetric top Hamiltonian to the much more highly resolved P and R branches (see Fig. 5).

vicinity of these modes would be quite high, which could in turn result in ubiquitous intensity borrowing, level shifts and perturbation of the rovibrational structure through intramolecular vibrational energy coupling (see ref. 9 for a detailed discussion of intramolecular vibrational distribution or IVR). By way of example of how this expectation is established, a much smaller hydrocarbon species such as 1-butyne has far fewer (24) vibrational modes, yet already exhibits a density of total vibrational states in the 3000–3300 cm^{-1} CH stretch region of 87 states per cm.[31] This is close to but lower than the critical threshold density of states, $\rho_{crit} \approx 100$ cm^{-1}, wherein each "zeroth order bright" state is within a typical hydrocarbon CH stretch coupling matrix element strength ($\langle \Psi_{dark}|H|\Psi_{bright}\rangle \approx 0.01$ cm^{-1}) of some state in the "dark" manifold. As a result, even under slit jet cooled conditions, the high resolution, sub-Doppler IR spectrum of 1-butyne shows dramatic spectral congestion due to unimolecular (IVR) coupling induced perturbations, with the oscillator strength of each rovibrational feature "split" into some 5–10 lines by mixing with nearby dark states.[31] If benzyl radical were to suffer IVR induced spectral congestion in proportion the number of modes, there would be essentially no isolated rovibrational transitions, which is not what we observed spectroscopically.

More quantitatively, we can estimate the benzyl radical density of states using the harmonic vibrational frequencies from DFT calculations and the backtracking algorithm of Kemper *et al.*[32] With all symmetry vibrational modes included, the harmonic density of states is estimated to be only 67 states cm^{-1} for a ± 5 cm^{-1} region centered on the ν_4 band origin, and 69 states per cm for a ± 5 cm^{-1} region centered on the ν_3 band origin. Obviously there will be smaller state densities if sorted by the corresponding irreducible representations for the C_{2v} group. Note that this estimate does not include any additional density due to asymmetry split levels coupled by Coriolis rovibrational interactions. Basically, the density of total vibrational states for benzyl radical in the CH stretch region is even lower than that of 1-butyne, despite benzyl radical's 1.5-fold more nuclei and therefore 50% more vibrational modes. Hence, somewhat surprisingly, the CH stretch spectra of benzyl radical, even at sub-Doppler (60 MHz) resolution, shows no direct evidence of strong vibrational mode coupling, intensity borrowing and/or level splitting.[33–35]

Though initially surprising, there are some precedents for such a lack of high resolution IVR structure in small aromatic hydrocarbon species.[36] The fundamental reason why benzyl radical with 36 vibrational modes has a smaller density of states than 1-butyne may be readily rationalized from simple elementary chemistry concepts. Benzyl is a resonantly stabilized aromatic species, with each of its CC bonds exhibiting partial double-bond character. The first excited state of the internal methylene hindered rotation is therefore anomalously high (500 cm^{-1}),[37] with a significant barrier to internal rotation, and as a result, much more vibrationally harmonic in character. By way of comparison, 1-butyne has a pair of nominally CC single bonds, each of which can exhibit nearly free internal rotation. The first excited state of the internal methyl hindered rotor in 1-butyne is therefore quite low (200 cm^{-1}) due to a much lower 1141 cm^{-1} rotational barrier,[38] and which combinatorially translates into a much higher density of states at comparable excitation energies. Stated in simple terms, aromatic delocalization of the π electron density around the ring makes benzyl radical vibrationally more rigid. Indeed, even the ν_3 and ν_4 CH stretch excited states observed in benzyl radical are still too low to exceed the energetic threshold to internal rotation (see Section IV-C). Thus, the methylene rotor acts as a "localized" vibrational mode (with quasi-harmonic spacings for low quantum numbers), whereas for 1-butyne, the highly perturbed CH acetylinic stretch progressions already lie far above the 1141 cm^{-1} internal rotor threshold. It is this energetic lack of access to the combinatorially rich density of states of a free CC single bond that makes the crucial difference.[33,34] This bodes well for extending such high resolution spectroscopic studies to other jet cooled, resonant stabilized ring radicals such as pyridyl, pyrazyl, naphthyl, cyclopentadienyl, and possibly even polycyclic aromatic hydrocarbon (PAH) species in the slit jet discharge expansion environment. Given the confirmation *via* near IR space telemetry of polyynes and the simplest of aromatic species (benzene) in protoplanetary nebula (viewed toward CRL 618) at the International Space Observatory,[39] the availability of such high resolution data for open shell aromatic hydrocarbons should provide multiple renewed opportunities for stimulating future astronomical searches.

C. *Ab initio* isomerization barrier and tunneling dynamics

Exchange of the two identical H atoms in the CH_2 internal rotor obviously does nothing to the potential energy of the radical, which implies that, for sufficiently low barrier heights, quantum mechanical tunneling can take place. An even more sensitive probe of the partial double bond character in the methylenic CH_2 rotor, and therefore the rigidity of the aromatic benzyl ring, can be provided by the presence (or absence) of

tunneling splitting effects in the high resolution spectra. From C_{2v} point group symmetry analysis, any spectral splittings observed on transitions in the A-type (ν_3) or B-type (ν_4) bands must reflect the difference ($\Delta\nu_{tun}' - \Delta\nu_{tun}''$) or sum ($\Delta\nu_{tun}' + \Delta\nu_{tun}''$), respectively, of tunneling splittings in the ground and excited states. We see no evidence for any such tunneling splitting or broadening of the lines in either the ν_3 or ν_4 band, from which we can place a rigorous upper limit of $\Delta\nu_{tun} = 0.001$ cm^{-1}. Indeed, the fits shown above are all based on assuming all tunneling splittings to be far smaller than the sub-Doppler resolution in the slit jet (60 MHz).

To better establish what that translates into as a quantitative estimate for the internal rotation barrier, we have pursued a combination of high level MOLPRO[40,41] and GAMESS[42,43] *ab initio* calculations for internal rotation of the methylenic CH_2 subunit. Specifically, we have first obtained the internal rotor barrier height ($\Delta E_{barrier}$ = 12.40 kcal mol^{-1} or 4337 cm^{-1}) by performing MOLPRO calculations at the C_{2v} global equilibrium and transition state geometries with explicitly correlated CCSD(T)-f12b methods in a Dunning correlation consistent cc-pV*n*Z (n = 2, 3) basis set and extrapolating to the CBS limit. Secondly, we have performed CCSD(T)-f12b/cc-pVdZ frequency calculations for both of these optimized geometries, which we can then use to estimate a zero-point corrected barrier height ($\Delta E_{barrier}$ = 11.45 kcal mol^{-1} = 4005 cm^{-1}) at the harmonic vibrational level. Finally, to characterize the shape of the potential well, we have used GAMESS methods to calculate the intrinsic reaction coordinate (IRC) ξ from the C_{2v} symmetry transition state down to the C_{2v} symmetry equilibrium planar geometry at the CCSD(T)/VDZ level, scaling the results to fit the ZPE corrected barrier height obtained at a much higher CCSD(T)-f12b/cc-pVD*n*Z-f12 (n = 2, 3) level and extrapolated to the complete basis set (CBS) limit.

The value of performing the GAMESS IRC calculations is that the reaction coordinate ξ can be obtained explicitly in mass weighted Cartesian ($a_0^{1/2}$ Å) units, *i.e.*, with no assumption required for rigid rotation of either the CH_2 or phenyl groups. The resulting Schroedinger equation can then be directly integrated using Numerov methods, with all effective reduced mass and moment of inertia information varying as a function of the IRC, which arises naturally from performing the calculation in mass weighted Cartesian coordinates. The resulting tunneling potential is presented in Fig. 7, with a sample tunneling wave function corresponding to 80% of the energy barrier and 24 quanta in the torsional coordinate. Despite the high number of quanta, the pair of tunneling state energies can be converged to high precision (1 part in 10^9) on this IRC potential by (i) using appropriate boundary condition (either $\psi(0) = 0$ or $d\Psi(0)/d\xi = 0$) at the equilibrium geometry and (ii) integrating away from the high transition state barrier to the equilibrium geometry to maintain numerical stability. The resulting tunneling splittings in the ground vibrational state for such a high barrier internal rotor potential are exceedingly small ($\approx$1 kHz or $\approx 1.0 \times 10^{-7}$ cm^{-1}), far below our sub-Doppler resolution limit, but with splittings growing to be as large as 3 GHz (0.1 cm^{-1}) for energies within a few hundred cm^{-1} of the 4337 cm^{-1} high internal rotation isomerization barrier.

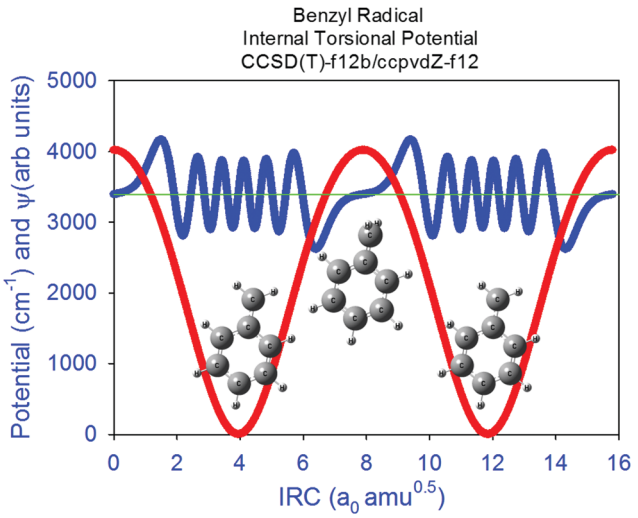

Fig. 7 Intrinsic reaction coordinate (IRC) and potential for internal rotation tunneling for benzyl radical. The barrier height (ΔE_{barr} = 12.40 kcal mol^{-1} = 4337 cm^{-1}) is obtained from Molpro CCSD(T)-f12b calculations of the transition state and equilibrium geometries at the cc-pv*n*Z-f12 (n = 2, 3) level and extrapolated to the CBS limit. This barrier is then corrected for the zero-point energy (ZPE) with Molpro CCSD(T)-f12b/cc-pVdZ-f12 frequency calculations (ΔE_{zpe} = 11.45 kcal mol^{-1} = 4005 cm^{-1}), with this ZPE corrected barrier height used to linearly scale the GAMESS calculations to achieve best estimation of the IRC potential in true mass weighted Cartesian coordinates. The wave function shown represents the ν = 24 torsional wavefunction at 3390.8 cm^{-1}, for which the tunneling splitting is still only $\Delta\nu_{tun}$ = 0.1 cm^{-1} = 3 GHz.

D. Rovibrational constants

The measured ground-state rovibrational constants can be usefully compared to a variety of experimental and computational results. For instance, the results are already in good agreement with the LIF results of Lin *et al.*[16] With theory, the agreement is less satisfactory but still quite reasonable. For example, equilibrium rotational constants computed at the DFT-B3LYP/6-311++g(3df,3pd) level yield A'' = 0.1859 cm^{-1}, and B'' = 0.09070 cm^{-1}, and C'' = 0.06090 cm^{-1}. There is less than 1% difference between our computed and measured rotational constants, with the theoretical A'' and B'' values disagreeing with experiment by only 3σ and 4σ, respectively. The disagreement between the C'' values is far more extreme (270σ), but largely a reflection of the much higher experimental precision. These calculations also yield harmonic band origins, which with an empirically benchmarked anharmonic correction[30] gives ν_3 = 3080 $\pm$ 10 cm^{-1} and ν_4 = 3086 $\pm$ 10 cm^{-1}. The computed band origins prove to be in very good agreement with experiment, indicating that DFT-B3LYP benchmark calculations for anharmonic correction factors produce satisfactory results for aromatic CH stretch modes that are in line with the wide variety of hydrocarbon radicals previously analyzed at high resolution by ref. 30.

Not surprisingly, the higher level MCSCF calculations are in better agreement with experimental results than are the DFT-B3LYP calculations, but the improvement is marginal. Table 1 lists the rotational constants predicted by MCSCF calculations. These values

differ from our measurements by only about 0.5%. The A'' values now disagree by 2σ and the B'' values disagree by 4σ. The difference in the C'' values is still much larger (150σ), due to the higher experimental precision.

As a final comment, the inertial defect[44] provides interesting additional clues about benzyl molecular geometry. The inertial defect, Δ, is defined as

$$\Delta = I_C - I_A - I_B \quad (1)$$

where the I_is are the moments of inertia along the three principal rotation axes. Normally, non-planar molecules have negative inertial defects ($I_C < (I_A + I_B)$) and planar molecules, for which $I_C \approx (I_A + I_B)$, have very small or slightly positive inertial defects. Coriolis coupling can strongly influence the size of the inertial defect for planar molecules, with coupling to in-plane and out-of-plane vibrational modes producing positive and negative contributions, respectively, as discussed elsewhere in detail.[45]

Inertial defects for benzyl radical for the ground state ($v = 0$) and the first-excited states ($v = 1$) for the ν_3 and ν_4 vibrational modes, computed from our measured rotational constants, are summarized in Table 3. The ground state value ($\Delta = 0.1 \pm 0.4$ amu Å^2) is statistically indistinguishable from zero, *i.e.*, in agreement with simple freshman chemistry expectations for a sp^2 hybridized methylene rotor and a coplanar aromatic ring, stabilized by resonance delocalization of the radical center and consistent with the LIF value of Lin *et al.*[9] ($\Delta = 0.02 \pm 0.11$ amu Å^2). The inertial defect computed from the CESE results of Fukushima and Obi ($\Delta = 0.5 \pm 0.2$ amu Å^2)[15] and the LIF results of Carrick and Selco ($\Delta = 0.64$ amu Å^2)[14] are somewhat larger, but still consistent with a planar geometry. Indeed, many single-ring, planar aromatic molecules have been shown to exhibit small positive inertial defects on the order of 0.05 amu Å^2 (for example, see Table 1 in Herschbach and Laurie[45]), which is in line with what we and Lin *et al.*[16] observe, though still well within 1σ uncertainty of zero. By way of contrast, the corresponding inertial defects for the excited vibrational states ($\Delta_3 = -0.6(3)$ amu Å^2 and $\Delta_4 = -0.25(13)$ amu Å^2) are negative, and likely reflect evidence for weak unimolecular coupling of the CH stretches to out-of-plane vibrational motion in the dark state vibrational manifold.

E. Combined analysis of the LIF/infrared data

Given the highly unsaturated nature of the bulk of the hydrocarbon radical species observed thus far *via* rotational astronomy, the probability of high densities of single ring, aromatic species such as benzene and benzyl radical in the interstellar medium seems quite probable. Although benzene is by far the lower energy species, its lack of any permanent dipole moment has rendered it challenging to view *via* rotational spectroscopy, though there have been low resolution spectra clearly obtained in the 14 μm mid IR region at the Infrared Space Observatory.[39] Hence, it will be in the detection of simple substituted and/or radicalized aromatics (*e.g.*, phenyl or benzyl radical) that further microwave evidence for aromatic ring formation in the interstellar medium will likely be firmly established. Such efforts, in turn, should be greatly facilitated by the availability of high precision rotational constants with which to guide an efficient spectral search.

We return briefly to the deviations between observed and 2-line ground state combination differences in Fig. 3 (predicted from previous spectroscopic analysis) which clearly reveal a very small but quite systematic trend with respect to the J rotational quantum number. This suggests that the rotational constants from the previous analysis could be improved with the current sub-Doppler resolution infrared spectra, which in turn can play a role in detection of interstellar benzyl radical *via* radio, microwave and/or mm-wave observational telescopes. In the interest of stimulating such studies, we have explored an alternative rotational analysis, this time to a combined list of 2-line ground state combination differences from both the LIF (see ref. 46 for the LIF values) and current high resolution IR studies, appropriately weighting the data in a non-linear least-squares program by the reciprocal variance (*i.e.*, $1/\sigma^2$) of the spectral measurements. More quantitatively, this translates into 4 : 1 relative weights for infrared *vs.* UV/visible LIF 2-line combination differences, with the IR data leveraged by the sub-Doppler nature of spectroscopy in the slit expansion.

The results of such a combined data fit are summarized in the final row of Table 1. The refitted values are in excellent agreement with the previous numbers reported by both the present work and Lin *et al.*,[16] however, with a significantly enhanced precision by combination of high resolution LIF and infrared data. It is our hope that these values will serve to facilitate first detection of jet cooled benzyl radical *via* conventional, laboratory based microwave spectroscopy in a supersonic expansion, which would then provide the requisite spectroscopic precision for facilitating future searches for benzyl radical in the interstellar medium.

Table 3 Inertial defects for the ground ($v = 0$) state and the first excited states ($v = 1$) of the ν_3 and ν_4 modes. Values are computed using the rotational constants measured for the present work. Units are in amu Å^2

Ground	ν_3	ν_4
0.1(4)	−0.6(3)	−0.25(13)

V. Summary and conclusion

High-resolution IR absorption spectroscopy of benzyl radical yields spectroscopic constants for the ground and first vibrationally-excited state of the ν_3 in-phase asymmetric stretch and the ν_4 in-phase symmetric stretch CH stretch modes in the phenyl ring. These measurements are undertaken with single-mode IR difference-frequency laser spectroscopy. A slit-discharge supersonic pulsed beam source generates jet cooled benzyl radicals in the gas phase through dissociative attachment of electrons to benzyl chloride. The supersonic expansion cools the radicals to $T_{rot} \approx 15$ K, providing an optimally high density of radicals per quantum state. High sensitivity is achieved with (i) laser-amplitude noise substraction (ii) phase sensitive detection, and (iii) a long absorption path length, with

the slit beam source providing inherent sub-Doppler linewidths (60 MHz), and a frequency reproducibility and accuracy of ±11 MHz and ±15 MHz, respectively.

With these methods, we have observed and assigned 117 P- and R-branch transitions for the ν_3 band and 94 P- and R-branch transitions for the ν_4 band (see ESI† for the complete line lists). The ground-state rotational constants are determined by exploiting transitions from both vibrational bands to fit 103 ground-state combination differences to a rigid asymmetric top Hamiltonian. Good agreement is found between our rotational constants and previously published values from LIF studies by Lin *et al.*[16] ($<1\sigma$). The first precision data on rotational constants and vibrational band origins for benzyl radical are determined for the ν_3 and ν_4 in-plane CH stretching modes. The inertial defect obtained for the vibrational ground state is completely consistent with a planar geometry, as expected from simple delocalization of the radical electron center around the aromatic ring. The calculated density of vibrational states and impact on the spectrum is much lower than might be anticipated for a 14-atom molecule with $\approx$3000 cm^{-1} excitation in the CH stretch manifold. Specifically, we see no detectable splittings or broadenings at our sub-Doppler resolution due to unimolecular "IVR coupling" with the manifold of near resonant bath vibrational states. This absence of spectral congestion can be rationalized on the basis of the structural rigidity arising from the resonantly stabilized aromatic ring, which in turn increases frequencies for the low-lying bending and twisting modes and dramatically reduces the effective density of vibrational states available for unimolecular interactions. We note that such results bode well for future studies of reactive jet cooled radicals with aromatic rings.

Furthermore, we have undertaken high level, explicitly correlated, coupled cluster calculations to estimate the influence of tunneling of the methylenic internal rotor on the high resolution spectrum, which predict that the barrier to internal rotation is approximately 4300 cm^{-1} (11 kcal mole^{-1}). By direct numerical integration of the Schroedinger equation along the intrinsic reaction coordinate path, we predict tunneling rates in the ground vibrational state too small to be experimentally resolved, as further confirmed by the absence of additional tunneling structure in the sub-Doppler infrared spectral measurements. The results are all in accord with simple freshman chemistry notions of resonance stabilized benzyl radical, with extensive electron delocalization around the aromatic ring framework and partial double bond character in the methylenic CC bond.

To provide the most precise ground-state rotational information, we have performed combined least squares fits on ground-state combination differences from both the IR and LIF data sets.[16] These constants will expedite successful spectroscopic detection of jet cooled benzyl radical by conventional earth-based microwave and radio-frequency methods, the precision constants from which should greatly facilitate spectroscopic search for benzyl radical in the interstellar medium.

Conflicts of interest

There are no conflicts to declare.

Acknowledgements

This work was supported by grants from the Department of Energy (DE-FG02-09ER16021 and DE-FG02-01ER14172 for DJN and TAM, respectively), with initial funds for construction of the slit-jet laser spectrometer provided by the National Science Foundation (CHE 1266416, PHY 1734006). We acknowledge support from the Ohio Supercomputer Center for computational work. We also would like to thank Professors Mark Gordon and Kirk Peterson for their generous help and support of our *ab initio* calculations based on GAMESS and MOLPRO software platforms, respectively.

References

1 A. Alexiou and A. Williams, *Combust. Flame*, 1996, **104**, 51.
2 P. R. Westmoreland, A. M. Dean, J. B. Howard and J. P. Longwell, *J. Phys. Chem.*, 1989, **93**, 8171.
3 M. Heaven, L. Dimauro and T. A. Miller, *Chem. Phys. Lett.*, 1983, **95**, 347.
4 N. M. Marinov, W. J. Pitz, C. K. Westbrook, M. J. Castaldi and S. M. Senkan, *Combust. Sci. Technol.*, 1996, **116**, 211.
5 D. Polino and M. Parrinello, *J. Phys. Chem. A*, 2015, **119**, 978.
6 S. Sinha and A. Raj, *Phys. Chem. Chem. Phys.*, 2016, **18**, 8120.
7 R. T. Morrison and R. N. Boyd, *Organic Chemistry*, Allyn and Bacon, Inc., Boston, 1979.
8 L. Pauling and G. W. Wheland, *J. Chem. Phys.*, 1933, **1**, 362.
9 D. J. Nesbitt and R. W. Field, *J. Phys. Chem.*, 1996, **100**, 12735.
10 T. W. Schmidt, *Int. Rev. Phys. Chem.*, 2016, **35**, 209.
11 H. Schuler, L. Reinebeck and R. Koberle, *Z. Naturforsch.*, 1952, **7**, 428.
12 G. Porter and E. Strachan, *Spectrochim. Acta*, 1958, **12**, 299.
13 C. Cossartmagos and S. Leach, *J. Chem. Phys.*, 1972, **56**, 1534.
14 P. G. Carrick and J. I. Selco, *J. Mol. Spectrosc.*, 1990, **139**, 449.
15 M. Fukushima and K. Obi, *J. Chem. Phys.*, 1992, **96**, 4224.
16 T. Y. D. Lin, X. Q. Tan, T. M. Cerny, J. M. Williamson, D. W. Cullin and T. A. Miller, *Chem. Phys.*, 1992, **167**, 203.
17 K. Tonokura and M. Koshi, *J. Phys. Chem. A*, 2003, **107**, 4457.
18 J. E. Rice, N. C. Handy and P. J. Knowles, *J. Chem. Soc., Faraday Trans.*, 1987, **83**, 1643.
19 E. G. Baskir, A. K. Maltsev, V. A. Korolev, V. N. Khabashesku and O. M. Nefedov, *Russ. Chem. Bull.*, 1993, **42**, 1438.
20 J. B. Kim, P. G. Wenthold and W. C. Lineberger, *J. Phys. Chem. A*, 1999, **103**, 10833.
21 S. Davis, M. Farnik, D. Uy and D. J. Nesbitt, *Chem. Phys. Lett.*, 2001, **344**, 23.
22 L. H. Deng, X. M. Gao, Z. S. Cao, W. D. Chen, Y. Q. Yuan, W. J. Zhang and Z. B. Gong, *Opt. Commun.*, 2006, **268**, 110.
23 M. J. Frisch, G. W. Trucks, H. B. Schlegel, G. E. Scuseria, M. A. Robb, J. R. Cheeseman, J. J. A. Montgomery, T. Vreven, K. N. Kudin, J. C. Burant, J. M. Millam, S. S. Iyengar, J. Tomasi, V. Barone, B. Mennucci, M. Cossi, G. Scalmani, N. Rega, G. A. Petersson, H. Nakatsuji, M. Hada, M. Ehara, K. Toyota, R. Fukuda, J. Hasegawa, M. Ishida, T. Nakajima, Y. Honda,

O. Kitao, H. Nakai, M. Klene, X. Li, J. E. Knox, H. P. Hratchian, J. B. Cross, C. Adamo, J. Jaramillo, R. Gomperts, R. E. Stratmann, O. Yazyev, A. J. Austin, R. Cammi, C. Pomelli, J. W. Ochterski, P. Y. Ayala, K. Morokuma, G. A. Voth, P. Salvador, J. J. Dannenberg, V. G. Zakrzewski, S. Dapprich, A. D. Daniels, M. C. Strain, O. Farkas, D. K. Malick, A. D. Rabuck, K. Raghavachari, J. B. Foresman, J. V. Ortiz, Q. Cui, A. G. Baboul, S. Clifford, J. Cioslowski, B. B. Stefanov, G. Liu, A. Liashenko, P. Piskorz, I. Komaromi, R. L. Martin, D. J. Fox, T. Keith, M. A. Al-Laham, C. Y. Peng, A. Nanayakkara, M. Challacombe, P. M. W. Gill, B. Johnson, W. Chen, M. W. Wong, C. Gonzalez and J. A. Pople, *Gaussian 09, Revision B.01*, Pittsburgh, PA, 2016.

24 E. Riedle, S. H. Ashworth, J. T. Farrell and D. J. Nesbitt, *Rev. Sci. Instrum.*, 1994, **65**, 42.

25 A. S. Pine, *J. Opt. Soc. Am.*, 1976, **66**, 97.

26 J. K. G. Watson, in *Vibrational Spectra and Structure*, ed. J. During, Elsevier, Amsterdam, 1977, vol. 6, p. 1.

27 S. C. Wang, *Phys. Rev.*, 1929, **34**, 243.

28 C. M. Western, *J. Quant. Spectrosc. Radiat. Transfer*, 2016, **186**, 221.

29 C. M. Western, *PGOPHER, a program for simulating rotational, vibrational, and electronic spectra*, Bristol University, 2016.

30 F. Dong, S. Davis and D. J. Nesbitt, *J. Phys. Chem. A*, 2006, **110**, 3059.

31 A. McLlroy and D. J. Nesbitt, *J. Chem. Phys.*, 1990, **92**, 2229.

32 M. J. H. Kemper, J. M. F. Vandijk and H. M. Buck, *Chem. Phys. Lett.*, 1978, **53**, 121.

33 G. A. Bethardy, X. L. Wang and D. S. Perry, *Can. J. Chem.*, 1994, **72**, 652.

34 A. McLlroy and D. J. Nesbitt, *J. Chem. Phys.*, 1994, **101**, 3421.

35 D. S. Perry, *J. Chem. Phys.*, 1993, **98**, 6665.

36 H. Li, C. C. Miller and L. A. Philips, *J. Chem. Phys.*, 1994, **100**, 8590.

37 Z. Li, T. Bally, K. N. Houk and W. T. Borden, *J. Org. Chem.*, 2016, **81**, 9576.

38 B. M. Landsberg and R. D. Suenram, *J. Mol. Spectrosc.*, 1983, **98**, 210.

39 J. Cernicharo, A. M. Heras, A. Tielens, J. R. Pardo, F. Herpin, M. Guelin and L. Waters, *Astrophys. J.*, 2001, **546**, L123.

40 H.-J. Werner, P. J. Knowles, G. Knizia, F. R. Manby and M. Schutz, *et al.*, *MOLPRO, version 2015.1, a package of ab intio programs*, 2015.

41 H.-J. Werner, P. J. Knowles, G. Knizia, F. R. Manby and M. Schutz, *Wiley Interdiscip. Rev.: Comput. Mol. Sci.*, 2012, **2**, 242.

42 M. W. Schmidt, K. K. Baldridge, J. A. Boatz, S. T. Elbert, M. S. Gordon, J. H. Jensen, S. Koseki, N. Matsunaga, K. A. Nguyen, S. Su, T. L. Windus, M. Dupuis and J. A. Montgomery, *Comput. Chem.*, 1993, **14**, 1347.

43 M. S. Gordon and M. W. Schmidt, in *Theory and applications of computational chemistry: the first forty years*, ed. C. E. Dykstra, G. Frenking, K. S. Kim, and G. E. Scuseria, Elsevier, Amsterdam, 2005, p. 1167.

44 T. Oka and Y. Morino, *J. Mol. Spectrosc.*, 1961, **6**, 472.

45 D. R. Herschbach and V. W. Laurie, *J. Chem. Phys.*, 1964, **40**, 3142.

46 A. J. Samin, *A statistical analysis of the rotational structure of the benzyl radical*, MS thesis, The Ohio State University, 2014.